CUNJIN LUO (Orcid ID : 0000-0003-3946-1093)

DR. TONG LIU (Orcid ID : 0000-0003-0482-0738)

Article type : Original Article

Cardiac abnormalities after induction of endoplasmic reticulum stress are associated with mitochondrial dysfunction and connexin43 expression

Jinli He MS [1#], Mengqi Gong MD, PhD [1,2#], Zaojia Wang MS[1], Daiqi Liu BS[1], Bingxin Xie BS[1], Cunjin Luo PhD [3], Guangping Li, MD, PhD [1], Gary Tse, PhD, FESC, FACC, FRCP [1,4,5*] and Tong Liu, MD, PhD[1 *]

1. Tianjin Key Laboratory of Ionic-Molecular Function of Cardiovascular disease, Department of Cardiology, Tianjin Institute of Cardiology, Second Hospital of Tianjin Medical University, Tianjin 300211, People's Republic of China

2. Department of Cardiology, The First Affiliated Hospital of Anhui Medical University, Hefei, China

3. School of Computer Science and Electronic Engineering, University of Essex, Colchester, CO4 3SQ, UK

4.Faculty of Health and Medical Sciences, University of Surrey, GU2 7AL, Guildford, United

Kingdom;

5.Kent and Medway Medical School, Canterbury, Kent, CT2 7NT, UK.

# The first two authors contributed equally to this work.

Running title: Endoplasmic reticulum stress (ERS) and cardiac dysfunction

***Corresponding Author**

Prof. Tong Liu

Tianjin Key Laboratory of Ionic-Molecular Function of Cardiovascular disease, Department of Cardiology, Tianjin Institute of Cardiology, Second Hospital of Tianjin Medical University, Tianjin 300211, People's Republic of China

Email: liutongdoc@126.com

Dr. Gary Tse

Tianjin Key Laboratory of Ionic-Molecular Function of Cardiovascular disease, Department of Cardiology, Tianjin Institute of Cardiology, Second Hospital of Tianjin Medical University, Tianjin 300211, People's Republic of ChinaEmail: gary.tse@doctors.org.uk

Keywords: ER stress, cardiac dysfunction, mitochondria CX43

Number of words: 5080

Data availability statement: Data available upon request.

Abstract

The endoplasmic reticulum (ER) is responsible for protein synthesis and calcium storage. ER stress, reflected by protein unfolding and calcium handling abnormalities, has been studied as a pathogenic factor in cardiovascular diseases. The aim of this study is to examine the effects of ER stress on mechanical and electrophysiological functions in the heart and explore the underlying molecular mechanisms.A total of 30 rats were randomly divided into control, ER stress inducer (tunicamycin) and ER stress inhibitor (tunicamycin+4-phenylbutyric acid, 4-PBA) groups. ER stress induction led to significantly systolic and diastolic dysfunction as reflected by maximal increasing/decreasing rate of left intraventricular pressure (±dp/dt), LV peak systolic pressure, LV development pressure and LV end-diastolic pressure. Epicardial mapping performed *in vivo* revealed reduced conduction velocity and increased conduction heterogeneity associated with the development of spontaneous ventricular tachycardia. Masson's trichrome staining revealed marked fibrosis in the myocardial interstitial and sub-pericardial regions, and thickened epicardium. Western blot analysis revealed increased pro-fibrotic factor TGF-β1, decreased mitochondrial biogenesis protein PGC-1a, decreased mitochondrial fusion protein MFN2. These changes were associated with mitochondria dysfunction and connexin 43 translocation to mitochondria. These abnormalities can be partially prevented by the ER stress inhibitor 4-PBA.Our study shows that ER stress induction can produce cardiac electrical and mechanism dysfunction as well as structural remodeling. Mitochondrial function alterations are contributed by CX43 transposition to mitochondria. These abnormalities can be partially prevented by the ER stress inhibitor 4-PBA.

1.Introduction

Cardiovascular disease is the major cause of mortality worldwide(1, 2). Emerging evidence points to the endoplasmic reticulum (ER) as an important organelle that contributes to the pathogenesis of different cardiovascular diseases (3), such as myocardial infarction and heart failure (4, 5). The ER functions as the protein handling machinery, responsible for the synthesis, folding, maturation and assembly of proteins before their export. When proteins are misfolded, ER stress and the unfolded protein response is elicited, leading to a protective mechanism in which protein synthesis is inhibited and the abnormal proteins are directed towards the removal pathways (6). This may induce apoptosis via mitochondrial-dependent and -independent mechanisms.

In this study, we i) examined the effects of the ER stress inducer, tunicamycin, on cardiac

structural, mechanical and electrophysiological function, ii) explored the underlying mechanisms involving mitochondrial function, and iii) investigated if the ER stress inhibitor 4-phenylbutyric acid (4PBA) can prevent all or some of these abnormalities.

2.Results

2.1 Tunicamycin and 4-PBA led to induction and inhibition of ER stress

An overview of the experiments conducted in this study is shown in **Figure 1A**. Injection of tunicamycin successfully induced ER stress as reflected by increased protein expression of CHOP (**Figure 1B**) and XBP-1 (**Figure 1C**). The protein levels were significantly reduced following injection of the ER stress inhibitor 4-PBA. No ultrastructural changes were observed in cardiomyocytes of control rats, with regular arrangement of myofibrils (mf) and mitochondria (m) (**Figure 1D**). Intermyofibrillar space was filled with the expansion of ER network in the tunicamycin group (**Figure 1E**). The ER network was not well-developed in the 4-PBA group (**Figure 1F**).

2.2 Transthoracic echocardiography, surface electrocardiography and hemodynamic measurements

The data from transthoracic echocardiography and surface electrocardiography are summarized in **Table 1**. None of the ECG parameters was altered by tunicamycin or 4-PBA. Left ventricular (LV) ejection fraction (EF) (**Figure 2A, left panel**) and fractional shortening (FS) (**Figure 2A, right panel**) were also not significantly altered by either tunicamycin or 4-PBA.

The systolic function parameters, LV contractility (+dp/dt) (**p=0.0494**) and LV peak systolic pressure (LVSP) (**p=0.0494**) were significantly lowered by tunicamycin (**Figure 2C**). For diastolic parameters, intraventricular pressure (-dP/dt) was significantly reduced (**P=0.0413**) whilst LV end-diastolic pressure (LVEDP) (**P=0.0494**) was significantly increased by tunicamycin (**Figure 2D**). These tended to be reversed by 4-PBA although the difference was not statistically significant (P>0.05,compared to tunicamycin group).

2.3 Epicardial electrophysiological mapping

Representative electrophysiological maps recorded from the epicardial surface *in vivo* are shown in **Figure 3A**. There was normal electrical conduction under control conditions (*left panel*) but slowed and heterogeneous conduction was observed after tunicamycin treatment (*middle panel*) and these abnormalities was only partially reversed by 4-PBA (*right panel*). Conduction velocity (CV) and conduction heterogeneity were quantified separately for the LV and right ventricle (RV). LV CV was significantly depressed (P=0.0151; **Figure 3B**) whilst LV inhomogeneity index (P=0.0075; **Figure 3C**) and LV inhomogeneity index normalized to the mean (P=0.0328; **Figure 3D**) were significantly higher for the tunicamycin group. Similar patterns of changes were observed for the CV measured at the RV (**Figure 3E**), RV inhomogeneity index (**Figure 3F**) and RV inhomogeneity index normalized to the mean (**Figure 3G**). These abnormalities were associated with the occurrence of spontaneous ventricular tachycardia (**Figure 3H to J**). Whilst 4-PBA failed to improve either CV or conduction heterogeneity in the LV and RV, spontaneous ventricular arrhythmias were not observed.

2.4 LV structural remodeling

LV posterior wall thickness in diastole (PWTd) (**Figure 4A**) and interventricular septum measured in diastole (IVSd) (**Figure 4B**) were not altered by either tunicamycin or 4-PBA. By histology, there was a higher percentage of LV fibrosis in the tunicamycin group compared to controls (P=0,0003; **Figure 4C**) and this was significantly reduced by 4-PBA (P=0.0003, compared to tunicamycin group; **Figure 4C**). The representative histological images are shown in **Figure 4D and 4E**. The white and black arrows denote interstitial fibrosis in the myocardium and sub-epicardium, respectively. Epicardial thickening is indicated by the red arrow. The pattern of changes in fibrosis is reflected by protein expression levels for TGF-β1 on Western blot analysis (**Figure 4F**).

2.5 Mitochondrial function and Cx43 expression

Mitochondrial respiratory function markers are shown in Figure 5A. In the TN group, state 3 respiration rate and respiratory control ratio (RCR) are statistically significant lowered compared with the control group. These changes were improved by 4PBA treatment. There is no significantly different of state 4 respiration rate among groups.

Mitochondrial membrane potential was determined by the ratio of red fluorescence to green fluorescence (**Figure 5B**). This was significantly reduced by tunicamycin (P=0.0224) and restored to control levels by 4-PBA (P=0.0338). Mitochondrial calcium content was quantified but no difference was detected among the three (**Figure 5C**).

Next, protein expression levels of important regulators of mitochondrial biogenesis were determined by Western blot analysis. The mitochondrial biogenesis-related protein (PGC-1α) (**Figure 5D**) and fusion-related protein (MFN2) (**Figure 5E**) were significantly downregulated by tunicamycin and this was not affected by 4-PBA treatment. Expression level of the mitochondrial fission protein (DRP1) was similar among three groups (**Figure 5F**).

Finally, a series of experiments were conducted to examine protein expression levels of Cx43 in the isolated mitochondria (**Figure 6A**). Mitochondrial Cx43 was significantly upregulated by tunicamycin (P=0.0151) and this was prevented by 4-PBA (P=0.0185, compared to the tunicamycin group). The relative protein expression of total Cx43 to mitochondrial Cx43 are shown in **Figure 6B**.

3. Discussion and Limitations

The main findings of this experimental study are that ER stress induction using tunicamycin led to partially cardiac dysfunction, reduced conduction velocity, increased conduction heterogeneity and spontaneous ventricular tachycardia. These were associated with marked

ventricular fibrosis, mitochondrial structural and functional abnormalities, increased protein expression of the pro-fibrotic factor TGF-β1, decreased expression of mitochondrial biogenesis protein PGC-1a and mitochondrial fusion protein MFN2, and probably increased connexin 43 translocation to mitochondria. Inhibition of ER stress using the agent 4-PBA prevented some of these abnormalities.

The main functions of the ER are protein synthesis, folding, maturation and assembly before further processing by the Golgi apparatus (3). Within the ER, there is a high oxidative stress environment, which promotes the formation of tertiary and quaternary structures of proteins. This is aided by chaperone proteins whose interactions with the proteins are facilitated by the luminal Ca^{2+} (7). Abnormalities in these processes can lead to misfolding or unfolding of proteins, which can accumulate within the ER lumen. This would promote ER stress, in turn eliciting the unfolded protein response (UPR) (8). UPR is a protective mechanism that slows the rate of protein synthesis, increases the folding ability of proteins and aids misfolded or unfolded protein to degradation pathways (6). The main regulators of the UPR are PERK, IRE1 and ATF6 (9). Prolonged ER stress leads to macrophage apoptosis associated with expression of the UPR sensor C/EBPα-homologous protein (CHOP), which also functions as a pro-apoptotic transcription factor. Together with XBP1, it is responsible for mitochondrial apoptotic pathway during prolonged or particularly severe ER stress (10). It is thought that acute or mild ER stress is protective whilst prolonged or severe ER stress is detrimental as apoptosis ensues. In the latter case, this is reflected by significantly upregulated XBP1 and CHOP. In this study, the agent tunicamycin was used for ER stress induction, as performed by other groups(11, 12). We observed conduction abnormalities in the form of slowed conduction and increased heterogeneity following prolonged ER stress induction. These changes can be explained by increased ventricular fibrosis promoted by increased TGF-β1. Moreover, we speculate that ion channel remodeling may contribute to abnormal conduction. Previous studies in other disease models have reported that PERK activation due to prolonged ER stress led to downregulation of the cardiac Na^{+} channels (13) as well as their inactivation resulting from Ca^{2+}/CaM binding to the IQ domain and phosphorylation of serine/threonine residues by CaMKII (14, 15). Moreover, Ca^{2+}-dependent activation of protein

kinase C (PKC) (16) can inactivate both Na^+ channels (17) and the gap junction protein Cx43 (18, 19). It is also possible that Ca^{2+} overload can lead to dephosphorylation of gap junctions (20), in turn resulting in their uncoupling (21) and lateralization (22, 23). Together, these electrophysiological remodeling can promote ventricular arrhythmias through reentrant mechanisms(24-26).

The ER has many membrane contact sites that connect it to other organelles especially the mitochondria(27). We explored the effects on mitochondrial function following ER stress activation. PGC-1α is an important protein that plays crucial functions in different aspects of mitochondrial biology. It acts as a transcription coactivator for PPAR-γ to regulate mitochondrial biogenesis, scavenges cellular ROS production by increasing Mn-SOD expression(28), and controls mitochondrial fusion and fission(29). Our group has previously explored abnormal mitochondrial function in diabetic rabbit models (30). Here we report that mitochondrial fusion protein MFN2 was decreased. Finally, the IP_3R1-GRP75-VDAC1 complex plays a major role in mediating calcium flow between the ER and the mitochondria especially during ER stress. The mitochondrial Cx43 plays important roles such as modulates mitochondrial respiration at respiratory complex I, production of radical oxygen species and ATP synthesis(31). Mitochondrial Ca^{2+} uptake from the ER lumen via the mitochondrial Cx43 can potentially lead to mitochondrial Ca^{2+} overload(32), cytochrome c release and apoptosis activation (33).

To test the hypothesis that reduction of ER stress can rescue the abnormal phenotype, we used the chemical chaperone 4-PBA (34), which can stabilize peptide structures and to improve the luminal folding capacity and traffic of aberrant proteins (35-37). This agent has previously demonstrated protective effects against apoptosis of cardiomyocytes by alleviating ER stress (38). We extend these findings by reporting that it can alleviate mechanical and electrical abnormalities following ER stress induction.

Several limitations of this study should be noted. Firstly, pharmacological agents were used to promote and inhibit ER stress, but non-specific effects cannot be excluded. Secondly, we conducted a comprehensive assessment of structural, mechanical and electrical function at the

systems level. Future experiments can explore the changes in ion channel function and expression that can explain the electrophysiological remodeling. Thirdly, intracellular Ca^{2+} handling, changes in the Ca^{2+}-dependent currents and Ca^{2+}-regulates proteins such as RyR2 were not assessed.

4.Materials and Methods

4.1 Animals and treatment protocol

This study received ethics approval from the Experimental Animal Administration Committee of Tianjin Medical University. A total of 30 male Sprague-Dawley, aged 8-week and weighed 190 - 210g, were adaptive feeding for 1 week and randomly divided into control, tunicamycin group and 4-PBA groups. Tunicamycin was dissolved by DMSO and diluted using saline, and injected via the intraperitoneal (i.p.) route (0.08mg/kg bid) for twice a week for 4 weeks. 4-PBA group was administered at 80 mg/kg/d; intra-gastrically (with equivalent i.p. dose tunicamycin calculated). Control group animals received i.p. injection 0.3-0.5 mL vehicle (DMSO+Saline). After 4-weeks, echocardiographic, hemodynamic and electrical mapping study were performed *in vivo*, and ventricular tissue were harvested for histopathology and molecular studies.

4.2 Echocardiography

Transthoracic echocardiography was performed in the supine position under isoflurane gas anesthesia after rats weighing. Echocardiographic views were obtained using the animal-oriented Doppler ultrasonic machine (SONICS, Newtown, CT, USA) and VisualSonicsVevo2100 imaging system. Left atrial (LA) anteroposterior diameter, left ventricular posterior wall thickness in diastole (LVPWTD), inter-ventricular septal thickness in diastole (IVSTd), left ventricular end-diastolic dimension(LVEDD), and left ventricular end-systolic dimension(LVESD) were measured using both 2-dimensional of LV long-axis views and M-mode imaging during 5 consecutive cardiac cycles. Left ventricular ejection fraction (LVEF) was calculated according to

the formula of EF (%) = (left ventricular end-diastolic volume - left ventricular end-systolic volume)/ (left ventricular end-diastolic volume)*100%.Left ventricular end-diastolic or end-systolic volume was calculated by Teichholtz formula ($V=7.0/ (2.4+D) \times D^3$; D represented as LVEDD or LVESD). The average of 3 measurements was calculated. Shortening fraction (SF, %) *(LVEDD－LVESD)/LVEDD*100.

4.3 Hemodynamic measurements and surface electrocardiographic (ECG) recordings

After echocardiographic assessment, rats of each group were anesthetized with 3% sodium pentobarbital (30 mg/kg) for right carotid artery isolating and cannulating to measure hemodynamic parameters during surface ECG monitoring with a BL-ICF biological function detection system (Chengdu Tai meng Science and Technology Co, Ltd). We firstly recorded stable electrocardiogram and blood pressure curve. Then we inserted the cannula through the aortic valve to the left ventricular to record the cardiac function curve. Finally, we selected 10 stable waveforms of electrocardiogram, blood pressure and cardiac function curve for analyzing parameters of heart rate, P wave duration, PR interval, QRS duration, QT interval, QTc interval, systolic pressure, diastolic pressure, LV peak systolic pressure (LVSP), LV end-diastolic pressure (LVEDP), and maximal increasing/decreasing rate of left intraventricular pressure (±dp/dt). Left ventricular development pressure (LVDP) was calculated by equation (LVDP= LVSP－LVEDP).

4.4 Electrophysiological mapping

Rats with stable vital signs at the end of hemodynamic assessment or direct anesthesia rats were selected to epicardial electrical mapping by positioning a 36-electrode microelectrode array (electrode impedance: 1.5 - 1.7Ω) on the epicardial surface of the left ventricular after thoracotomy in vivo. Inhomogeneity index, absolute inhomogeneity, and mean conduction velocity of inter-electrode were calculated. We chose the pictures with the same conduction direction for analysis and calculation(39, 40).We obtained data and pictures by multi-channel

systems (EMS64-USB-1003, United Kingdom) and EMapScope software provided by Mapping Lab.

4.5 Sample collection

The hearts were then immediately separated and weighed for recording.LV tissue for molecular biology study were frozen immediately in liquid nitrogen and stored at -80°C. Small pieces of LV tissue were fixed in 5- time-volume 10%formaldehyde for Masson-trichrome staining and fixed in 5- time-volume 2.5% glutaraldehyde for cardiac ultrastructural observations..

4.6 Extraction of mitochondria from ventricular myocardium

Each rat weighed 200 mg fresh LV tissue to extract mitochondria within 1 hour according to the kit (SM0020, Beijing Solar Bioscience & Technology Co., Ltd). Extracted mitochondria were stored in the specific storage solution in the kit and used for experimentation immediately after preparation.

4.7 Mitochondrial membrane potential measurements

The JC-1 probe is a sensitive fluorescent dye used to detect mitochondrial membrane potential. Red fluorescence of JC-1 represented mitochondria membrane potential increase. Green fluorescence, reflecting the monomeric form of JC-1, showed mitochondrial membrane decrease. Mitochondrial membrane potential changes were evaluated by measuring the ratio of red fluorescence and green fluorescence stained by JC-1 (C2006, Beyotime Biotechnology). Purified mitochondria were incubated with JC-1 for 20 min at 37 °C in the dark and washed stained-mitochondria with PBS buffer then by centrifugation for mitochondria collection(41). Mitochondrial membrane potential immediately was assessed by detecting CY3 (red) fluorescence and FLUO4 (green) fluorescence with fluorescence enzyme-labeled instrument.

4.8 Quantification of mitochondrial respiration function

Mitochondrial respiratory function was measured polarographically at 25 ℃ using a Clark-type oxygen electrode (Oroboros Instruments, Innsbruck, Austria). After a standardized instrumental and chemical calibration, 300 ug of mitochondrial protein was added to the reaction system. Upon stabilization of the mitochondrial oxygen consumption, a 20 uL mixture of 0.8 mol/L malic acid and 1 mol/L glutamic acid was added to initiate state 2 respiration. After stable state 2 respiration was established, state 3 respiration was initiated by the addition of 20uL 0.5 mol/L adenosine diphosphate (ADP, 0.5mM). When all of the ADP had been phosphorylated to adenosine triphosphate (ATP), the respiratory rate returned to state 4. The respiratory control ratio was calculated as the ratio of state 3 to state 4 respiratory rate.

4.9 Mitochondrial calcium overload measurements

Mitochondrial protein was quantified using the BCA protein assay reagent kit (Thermo Scientific). Three freeze-thaw cycles from room temperature to -80 °C were applied to release Ca^{2+} from the inner-mitochondria. Calcium content of 40μL mitochondria was calculated using the Calcium Assay Kit (C004-2, Nanjing Jiancheng Engineering Institute) and expressed as mmol/μg.

4.10 Histological and ultrastructural analyses

The LV tissue was cut into 5μm slices after dehydration and embedding and stained Masson's trichrome staining to evaluate the extent of fibrosis. At least 5 slices were stained for each one rat, each stained-slice was randomly photographed 3 high power fields (magnification, 400×) with excluding blood vessels sections and epicardium were separately photographed (magnification, 100×). The extent of interstitial fibrosis was evaluated by the blue pixel content of the digitized images than the total tissue area using Image-Pro Plus 6.0 Scion image software (Scion Corporation). LV tissues, fixated in 2.5% glutaraldehyde, were used for ultra-structural

analysis. Ultrathin slices were cut after further fixing in 1% osmium tetroxide, dehydrating in ethanol, and embedding in epon. The myocardial ultrastructure was observed under H-7650 transmission electron microscope (Hitachi).

4.11Western blot analysis

Frozen tissues were weighed, grinded on the ice plate and lysed for 30 min at 4℃ in RIPA lysis buffer plus a protease inhibitor of PMSF. The lysates were centrifuged at 14 000rpm for 15 minutes, and the supernatants were collected. The protein concentration evaluated using BCA protein assay reagent kit (Thermo Scientific). Proteins were separated on SDS-PAGE gels and transferred to polyvinylidene difluoride (PVDF) membranes (Millipore) and cut membranes were separately incubated overnight at 4 ℃ with specific primary antibody of CHOP (1:1000;#2895,CellSignaling),XBP-1(1:1000;ab37152),TGF-β1(1:1000;ab190503),PGC-1a(1:1000;ab54481)),MFN2(1:1000;ab56889),DRP1(1:1000;ab5678),CX43(1:1000;ab11370),β-actin(1:5000;60008-1-Ig,Proteintech) after sealing in 5%milk for 1 hour at room temperature ,then incubated with corresponding peroxidase-conjugated secondary antibodies. The reactions were visualized with Western Lightning Chemiluminescence Reagent (Millipore). The results were observed with auto radiographic film (Fujifilm Holdings Corp).

For mitochondrial-related proteins, the mitochondria were lysed in RIPA lysis buffer plus a protease inhibitors of PMSF for 30min at 4℃.Then mitochondrial protein was performed western blot analysis consistent with the above process for protein of CX43 (1:2000;ab11370), VDAC1(1:1000;ab14734) and β-actin (1:5000;60008-1-Ig,Proteintech).

4.12 Statistical analysis

All data are presented as mean ± SEM. Statistical analyses and image output were performed with GraphPad Prism software (Version 7, USA). Normal distribution was assessed using Kolmogorov-Smirnov test. Differences were assessed by one-way ANOVA or equivalent

nonparametric tests for normally and non-normally distributed data. Two-tailed $p < 0.05$ was considered statistically significant.

ACKNOWLEDGEMENTS

This study was supported by grants from the Tianjin Natural Science Foundation (grant no. 20JCZDJC00340 to T.L.) and National Natural Science Foundation of China.[grant no. 81970270 to T.L.]. And the English language edit from Dr. Gary Tse.

References

1. Benjamin EJ, Blaha MJ, Chiuve SE, et al. Heart Disease and Stroke Statistics-2017 Update: A Report From the American Heart Association. *Circulation* 2017; **135**:e146-e603.

2. Dharmarajan K, Li J, Li X, Lin Z, Krumholz HM, Jiang L. The China Patient-Centered Evaluative Assessment of Cardiac Events (China PEACE) retrospective study of acute myocardial infarction: study design. *Circulation. Cardiovascular quality and outcomes* 2013; **6**:732-40.

3. Minamino T, Kitakaze M. ER stress in cardiovascular disease. *Journal of molecular and cellular cardiology* 2010; **48**:1105-10.

4. Li S, Ma J, Li JB, et al. Over-expression of calpastatin attenuates myocardial injury following myocardial infarction by inhibiting endoplasmic reticulum stress. *Journal of thoracic disease* 2018; **10**:5283-97.

5. Okada K, Minamino T, Tsukamoto Y, et al. Prolonged endoplasmic reticulum stress in hypertrophic and failing heart after aortic constriction: possible contribution of endoplasmic reticulum stress to cardiac myocyte apoptosis. *Circulation* 2004; **110**:705-12.

6. Tsang KY, Chan D, Bateman JF, Cheah KS. In vivo cellular adaptation to ER stress: survival strategies with double-edged consequences. *Journal of cell science* 2010; **123**:2145-54.

7. Kim I, Xu W, Reed JC. Cell death and endoplasmic reticulum stress: disease relevance and therapeutic opportunities. *Nature reviews. Drug discovery* 2008; **7**:1013-30.

8. Bertolotti A, Zhang Y, Hendershot LM, Harding HP, Ron D. Dynamic interaction of BiP and ER stress transducers

in the unfolded-protein response. *Nature cell biology* 2000; **2**:326-32.

9. Iurlaro R, Munoz-Pinedo C. Cell death induced by endoplasmic reticulum stress. *The FEBS journal* 2016; **283**:2640-52.

10. Senft D, Ronai ZA. UPR, autophagy, and mitochondria crosstalk underlies the ER stress response. *Trends in biochemical sciences* 2015; **40**:141-8.

11. Shen M, Wang L, Guo X, et al. A novel endoplasmic reticulum stressinduced apoptosis model using tunicamycin in primary cultured neonatal rat cardiomyocytes. *Mol Med Rep* 2015; **12**:5149-54.

12. Qi X, Vallentin A, Churchill E, Mochly-Rosen D. deltaPKC participates in the endoplasmic reticulum stress-induced response in cultured cardiac myocytes and ischemic heart. *Journal of molecular and cellular cardiology* 2007; **43**:420-8.

13. Gao G, Xie A, Zhang J, et al. Unfolded protein response regulates cardiac sodium current in systolic human heart failure. *Circulation. Arrhythmia and electrophysiology* 2013; **6**:1018-24.

14. Ashpole NM, Herren AW, Ginsburg KS, et al. Ca2+/calmodulin-dependent protein kinase II (CaMKII) regulates cardiac sodium channel NaV1.5 gating by multiple phosphorylation sites. *The Journal of biological chemistry* 2012; **287**:19856-69.

15. Tan HL, Kupershmidt S, Zhang R, et al. A calcium sensor in the sodium channel modulates cardiac excitability. *Nature* 2002; **415**:442-7.

16. Luo JH, Weinstein IB. Calcium-dependent activation of protein kinase C. The role of the C2 domain in divalent cation selectivity. *The Journal of biological chemistry* 1993; **268**:23580-4.

17. Qu Y, Rogers JC, Tanada TN, Catterall WA, Scheuer T. Phosphorylation of S1505 in the cardiac Na+ channel inactivation gate is required for modulation by protein kinase C. *The Journal of general physiology* 1996; **108**:375-9.

18. Moreno AP, Sáez JC, Fishman GI, Spray DC. Human connexin43 gap junction channels. Regulation of unitary conductances by phosphorylation. *Circulation research* 1994; **74**:1050-7.

19. Kwak BR, Hermans MM, De Jonge HR, Lohmann SM, Jongsma HJ, Chanson M. Differential regulation of distinct types of gap junction channels by similar phosphorylating conditions. *Molecular biology of the cell* 1995; **6**:1707-19.

20. Huang XD, Sandusky GE, Zipes DP. Heterogeneous loss of connexin43 protein in ischemic dog hearts. *Journal of cardiovascular electrophysiology* 1999; **10**:79-91.

21. Beardslee MA, Lerner DL, Tadros PN, et al. Dephosphorylation and intracellular redistribution of ventricular

connexin43 during electrical uncoupling induced by ischemia. *Circulation research* 2000; **87**:656-62.

22. Smith JH, Green CR, Peters NS, Rothery S, Severs NJ. Altered patterns of gap junction distribution in ischemic heart disease. An immunohistochemical study of human myocardium using laser scanning confocal microscopy. *The American journal of pathology* 1991; **139**:801-21.

23. Lampe PD, TenBroek EM, Burt JM, Kurata WE, Johnson RG, Lau AF. Phosphorylation of connexin43 on serine368 by protein kinase C regulates gap junctional communication. *The Journal of cell biology* 2000; **149**:1503-12.

24. Tse G, Yeo JM. Conduction abnormalities and ventricular arrhythmogenesis: The roles of sodium channels and gap junctions. *International journal of cardiology. Heart & vasculature* 2015; **9**:75-82.

25. Tse G, Lai ET, Lee AP, Yan BP, Wong SH. Electrophysiological Mechanisms of Gastrointestinal Arrhythmogenesis: Lessons from the Heart. *Frontiers in physiology* 2016; **7**:230.

26. Tse G, Lai ETH, Yeo JM, Tse V, Wong SH. Mechanisms of electrical activation and conduction in the gastrointestinal system: lessons from cardiac electrophysiology. *Frontiers in Physiology* 2016; **7**.

27. Phillips MJ, Voeltz GK. Structure and function of ER membrane contact sites with other organelles. *Nature reviews. Molecular cell biology* 2016; **17**:69-82.

28. Fujisawa K, Nishikawa T, Kukidome D, et al. TZDs reduce mitochondrial ROS production and enhance mitochondrial biogenesis. *Biochemical and biophysical research communications* 2009; **379**:43-8.

29. Dabrowska A, Venero JL, Iwasawa R, et al. PGC-1alpha controls mitochondrial biogenesis and dynamics in lead-induced neurotoxicity. *Aging (Albany NY)* 2015; **7**:629-47.

30. Zhang X, Zhang Z, Zhao Y, et al. Alogliptin, a Dipeptidyl Peptidase-4 Inhibitor, Alleviates Atrial Remodeling and Improves Mitochondrial Function and Biogenesis in Diabetic Rabbits. *Journal of the American Heart Association* 2017; **6**.

31. Rodriguez-Sinovas A, Ruiz-Meana M, Denuc A, Garcia-Dorado D. Mitochondrial Cx43, an important component of cardiac preconditioning. *Biochimica et biophysica acta. Biomembranes* 2018; **1860**:174-81.

32. Gadicherla AK, Wang N, Bulic M, et al. Mitochondrial Cx43 hemichannels contribute to mitochondrial calcium entry and cell death in the heart. 2017; **112**:27.

33. Vannuvel K, Renard P, Raes M, Arnould T. Functional and morphological impact of ER stress on mitochondria. *Journal of cellular physiology* 2013; **228**:1802-18.

34. Kolb PS, Ayaub EA, Zhou W, Yum V, Dickhout JG, Ask K. The therapeutic effects of 4-phenylbutyric acid in

maintaining proteostasis. *The international journal of biochemistry & cell biology* 2015; **61**:45-52.

35. Jian L, Lu Y, Lu S, Lu C. Chemical chaperone 4-phenylbutyric acid protects H9c2 cardiomyocytes from ischemia/reperfusion injury by attenuating endoplasmic reticulum stress-induced apoptosis. *Molecular medicine reports* 2016; **13**:4386-92.

36. Li P, Zhang L, Zhang M, Zhou C, Lin N. Uric acid enhances PKC-dependent eNOS phosphorylation and mediates cellular ER stress: A mechanism for uric acid-induced endothelial dysfunction. *International journal of molecular medicine* 2016; **37**:989-97.

37. Roy D, Kumar V, James J, et al. Evidence that Chemical Chaperone 4-Phenylbutyric Acid Binds to Human Serum Albumin at Fatty Acid Binding Sites. *PloS one* 2015; **10**:e0133012.

38. Zhang C, Tang Y, Li Y, et al. Unfolded protein response plays a critical role in heart damage after myocardial ischemia/reperfusion in rats. *PloS one* 2017; **12**:e0179042-e.

39. Lammers WJ, Schalij MJ, Kirchhof CJ, Allessie MA. Quantification of spatial inhomogeneity in conduction and initiation of reentrant atrial arrhythmias. *The American journal of physiology* 1990; **259**:H1254-63.

40. Mollenhauer M, Friedrichs K, Lange M, et al. Myeloperoxidase Mediates Postischemic Arrhythmogenic Ventricular Remodeling. *Circulation research* 2017; **121**:56-70.

41. Renault TT, Luna-Vargas MP, Chipuk JE. Mouse Liver Mitochondria Isolation, Size Fractionation, and Real-time MOMP Measurement. *Bio-protocol* 2016; **6**.

Figure Legends

Figure 1. (A) Overview of the experiments conducted in this study: Aged 8-week SD rats were adaptive feeding for 1 week and then were randomly assigned to control, TN group and 4-PBA group. Control group animals received i.p. (intraperitoneal) injection 0.3-0.5 mL vehicle (DMSO+Saline).Tunicamycin was dissolved by DMSO and diluted using saline, and injected via the i.p. route (0.08mg/kg bid) for twice a week for 4 weeks in TN group and 4-PBA group. 4-PBA group was additionally administered 4-PBA at 80 mg/kg/d intra-gastrically (i.g).(B) Protein expression of CHOP. (C) Protein expression of XBP1. Quantification were relative to β-actin control. (D-F)Ultrastructural changes among three groups. TN: tunicamycin; 4PBA: 4-phenylbutyric acid; mf: myofibrils; m: mitochondria; short arrows: branches of rough ER; Long arrows: smooth SR vesicles. Results are represented as mean ± SEM. *P < 0.05; **P < 0.01; ***P < 0.001 (one-way ANOVA). **Figure 2.** (A) Ejection fraction (EF) and fractional shortening (FS). (B) Representative traces of hemodynamic measurements along with the surface electrocardiograms. (C) Systolic function parameters (+dP/dt: maximal increasing rate of left intraventricular pressure; LVSP, left ventricular systolic pressure; LVDP: Left ventricular development pressure; Systolic blood pressure). (D) Diastolic function parameters (-dP/dt, maximal decreasing rate of left intraventricular pressure; LVEDP, left ventricular end-diastolic pressure). TN: tunicamycin; 4PBA: 4-phenylbutyric acid. Results are represented as mean ± SEM. * denotes P<0.05.

Figure 3. (A) Representative electrophysiological maps recorded from the epicardial surface in vivo. (B) Left ventricular conduction velocity (LVCV), (C) inhomogeneity index and (D) inhomogeneity index relative to the mean. (E) Right ventricular conduction velocity (RVCV), (F) inhomogeneity index and (G) inhomogeneity index relative to the mean. (H) Spontaneous ventricular tachycardia recorded by 36-electrode microelectrode (red arrow: ventricular tachycardia; black arrow: normal beats). (I) LV and (J) RV recordings. TN: tunicamycin; 4PBA: 4-phenylbutyric acid. Results are represented as mean ± SEM. *P < 0.05; **P < 0.01(one-way ANOVA for normal distribution and nonparametric test for non-normal distribution).

Figure 4. (A) LV posterior wall thickness (PWTd) and (B) interventricular septum in diastole.

(C) % LV fibrosis. (D) Representative photographs of left ventricular interstitial fibrosis using Masson's trichrome staining (white arrow: blue collagen fibers; 400X). (E) Representative photographs of the epicardium using Masson's trichrome staining (black arrow: blue collagen fibers; red arrow: epicardial; 100X). (F) TGF-β1 protein expression by Western blot. TN: tunicamycin; 4PBA: 4-phenylbutyric acid. Results are represented as mean ± SEM. *P < 0.05; ***P<0.001(one-way ANOVA for normal distribution and nonparametric test for non-normal distribution).

Figure 5. (A) Mitochondrial respiratory function markers are shown..RCR: respiratory control ratio .(B) Mitochondrial membrane potential calculated by the ratio of red fluorescence to green fluorescence (red fluorescence: CY3; green fluorescence: FLUO4). (C) Mitochondrial calcium content expressed as unit of mmol/μg among three groups by a Calcium Assay Kit. Western plots of (D) PGC-1α, (E) MFN2 and (F) DRP1. TN: tunicamycin; 4PBA: 4-phenylbutyric acid. Results are represented as mean ± SEM. *P <0.05; **P<0.01(one-way ANOVA for normal distribution and nonparametric test for non-normal distribution).

Figure 6. (A) Mitochondrial Cx43 protein expression. (B) The relative protein expression of total Cx43 to mitochondria Cx43. TN: tunicamycin; 4PBA: 4-phenylbutyric acid. Results are represented as mean ± SEM. *P <0.05; **P<0.01(one-way ANOVA).

Table1. Echocardiographic and electrocardiographic parameters.

Echocardiographic parameters	Control Group(n=8)	TN Group(n=8)	4PBAGroup(n=8)
LAD, mm	3.62±0.10	3.82±0.16	3.58±0.06
LVESD, mm	4.75±0.41	4.63±0.13	4.46±0.09
LVEDD, mm	7.84±0.25	7.23±0.13*	7.24±0.08
Heart weight ratio (1/1000)	3.33±0.16	3.35±0.14	3.39±0.22
LV weight ratio (1/1000)	2.25±0.08	2.28±0.06	2.39±0.17
Ectrocardiographic parameters	Control Group(n=8)	TN Group(n=8)	4PBAGroup(n=8)
HR, bpm	430.30±13.05	422.40±6.14	413.30±23.41
MBP, mm Hg	132.50±4.06	124.40±6.44	118.30±7.21
PP, mm Hg	27.50±1.45	25.51±2.14	31.46±1.00
PR interval(ms)	44.57±1.37	43.58±2.35	47.66±1.40
P wave duration(ms)	14.81±0.70	14.42±1.37	16.37±0.99
QRS duration(ms)	19.82±1.13	20.90±2.38	15.90±0.65
QT interval(ms)	68.42±6.52	69.31±6.85	72.58±7.15
QTC interval(ms)	182.90±17.26	183.90±18.54	188.90±15.56

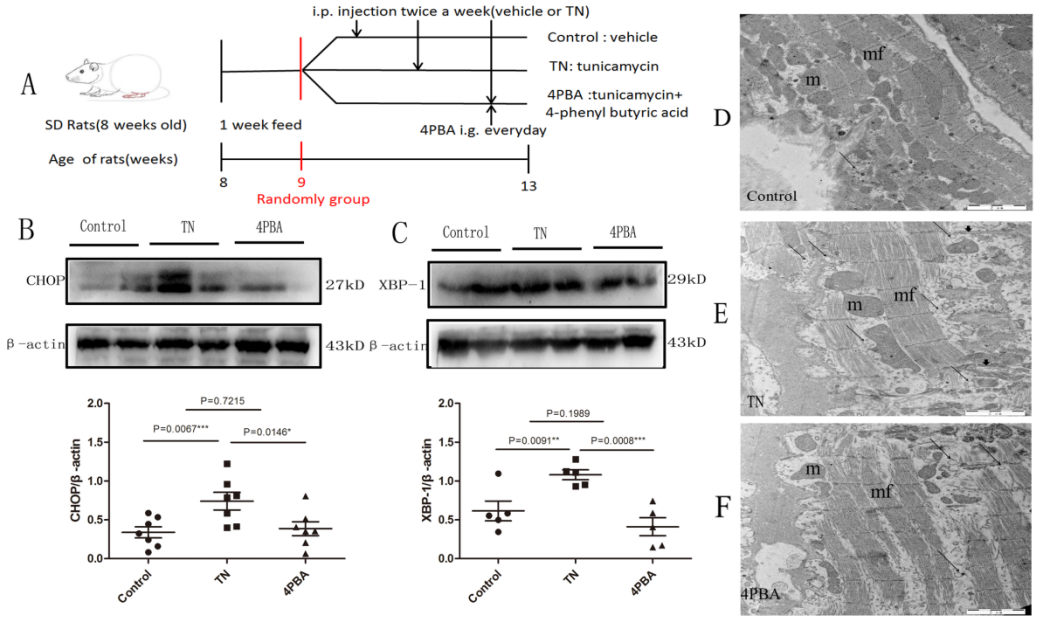

cep_13541_f1.tif

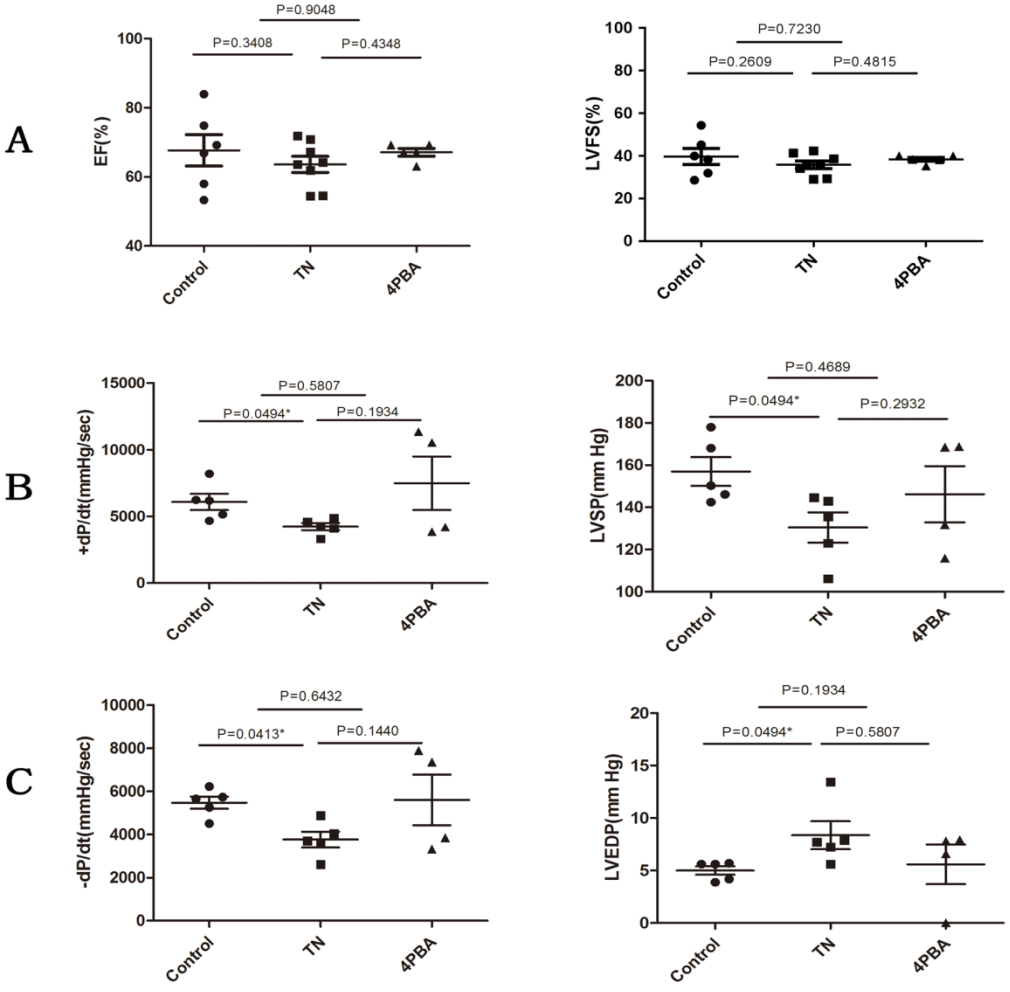

cep_13541_f2.tif

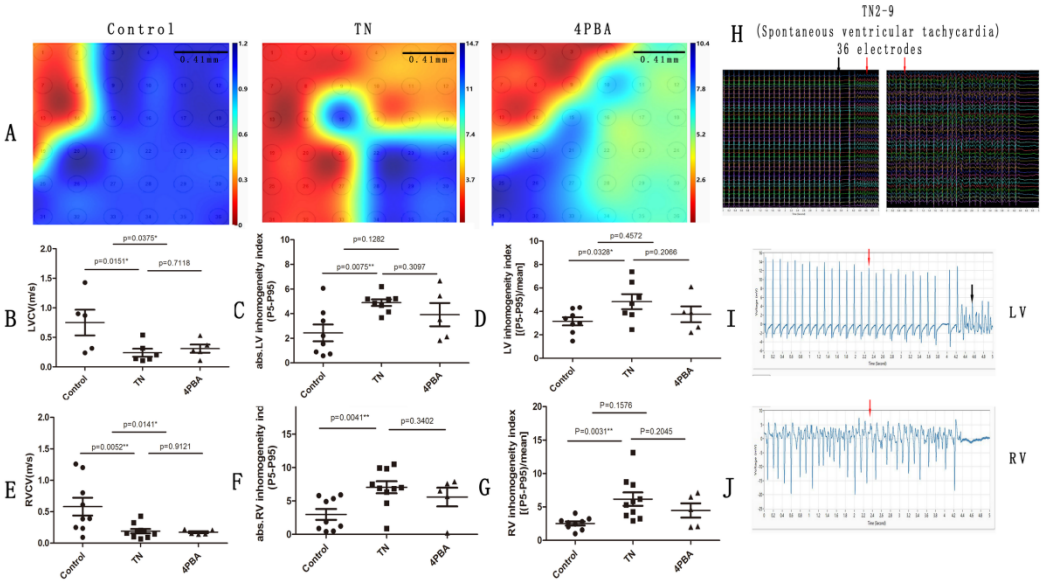

cep_13541_f3.tif

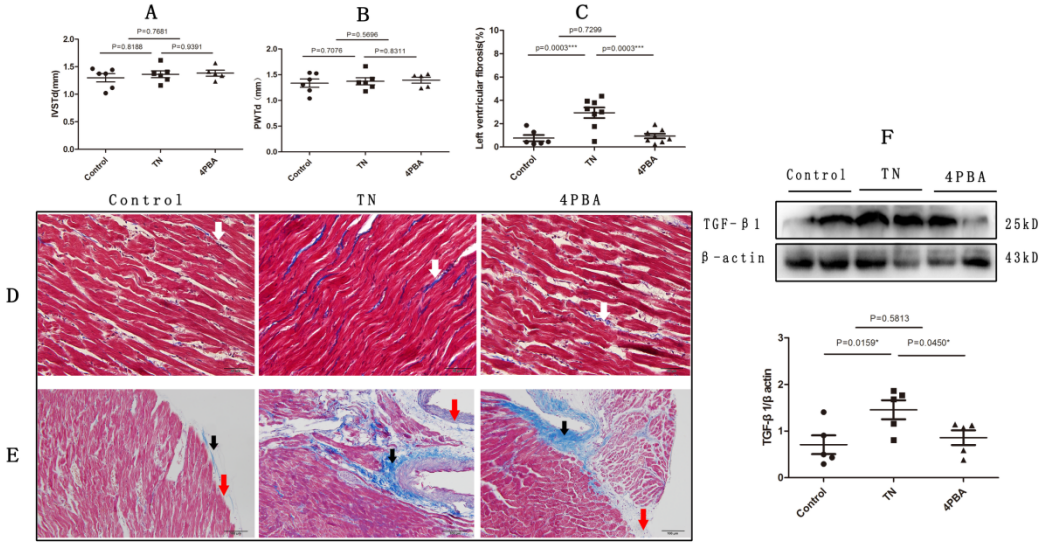

cep_13541_f4.tif

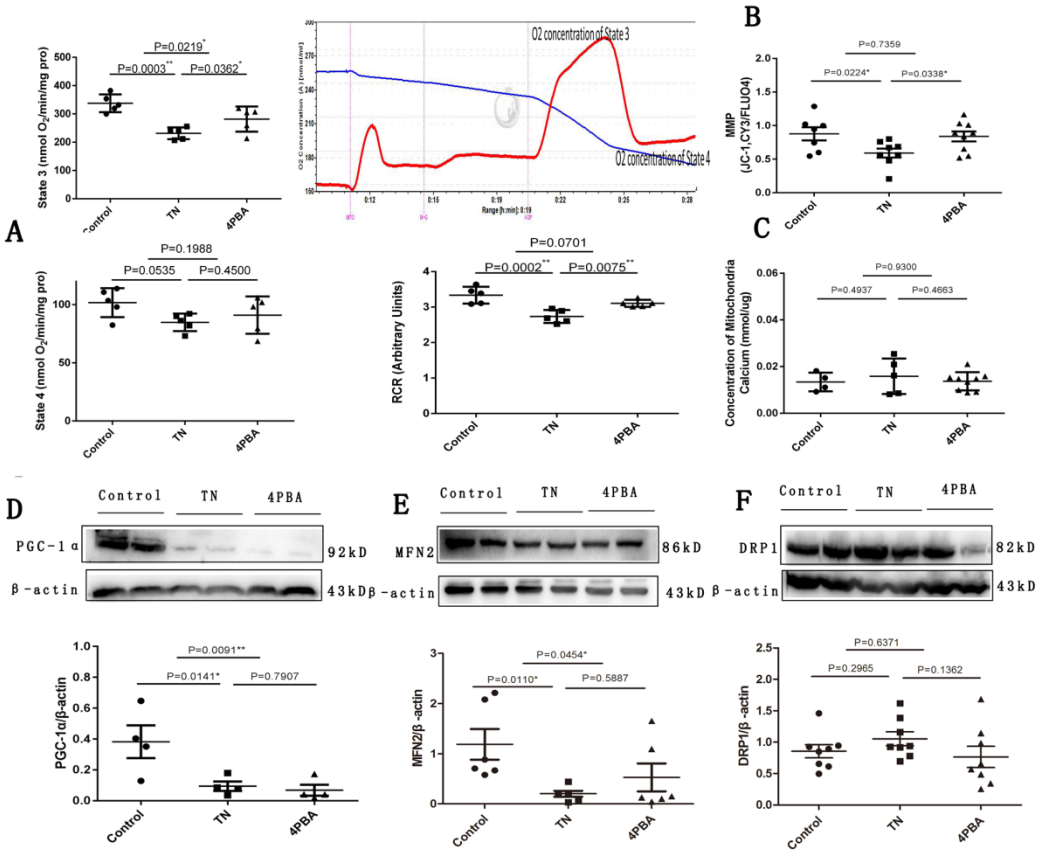

cep_13541_f5.tif

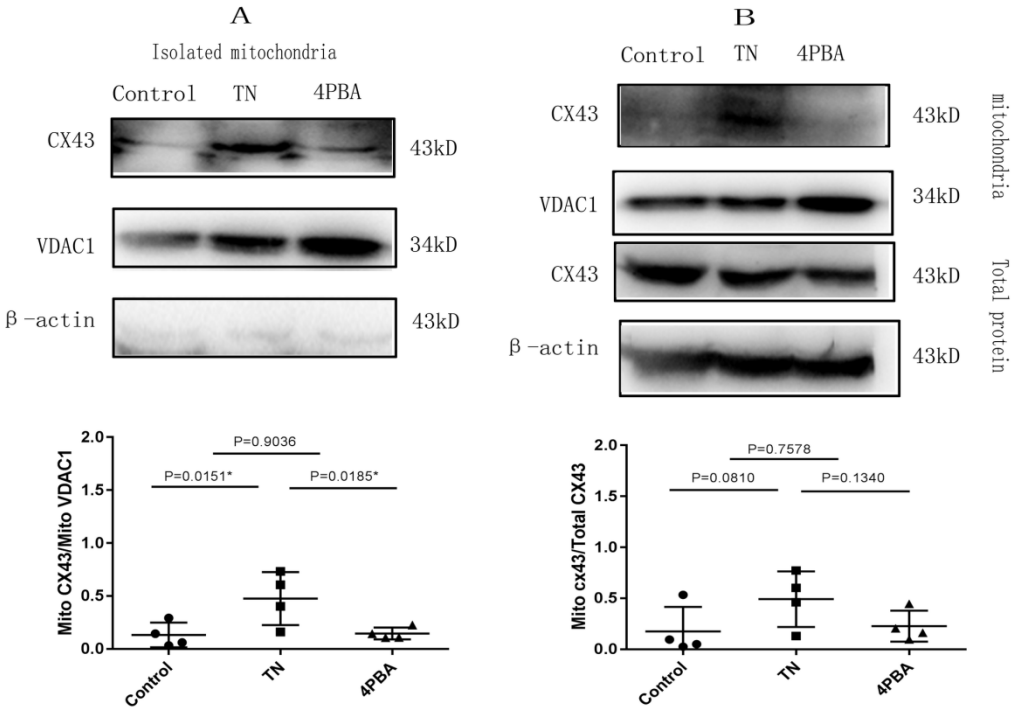

cep_13541_f6.tif